Solution precursor synthesis and magnetic properties of $Eu_{1-x}Ca_xTiO_3$

Nathaniel L. Henderson [a], Xianglin Ke [b,c], Peter Schiffer [b,c], Raymond E. Schaak [a,c,*]

[a] Department of Chemistry, The Pennsylvania State University, University Park, PA 16802, USA
[b] Department of Physics, The Pennsylvania State University, University Park, PA 16802, USA
[c] Materials Research Institute, The Pennsylvania State University, University Park, PA 16802, USA

ARTICLE INFO

ABSTRACT

Europium titanate, $EuTiO_3$, is a paraelectric/antiferromagnetic cubic perovskite with $T_N=5.5$ K. It is predicted that compressive strain could induce simultaneous ferroelectricity and ferromagnetism in this material, leading to multiferroic behavior. As an alternative to epitaxial strain, we explored lattice contraction via chemical substitution of Eu^{2+} with the smaller Ca^{2+} cation as a mechanism to tune the magnetic properties of $EuTiO_3$. A modified sol–gel process was used to form homogeneously mixed precursors containing Eu^{3+}, Ca^{2+}, and Ti^{4+}, and reductive annealing was used to transform these precursors into crystalline powders of $Eu_{1-x}Ca_xTiO_3$ with $x=0.00$, 0.05, 0.10, 0.15, 0.25, 0.35, 0.50, 0.55, 0.60, 0.65, 0.80, and 1.00. Powder XRD data indicated that a continuous $Eu_{1-x}Ca_xTiO_3$ solid solution was readily accessible, and the lattice constants agreed well with those predicted by Vegard's law. SEM imaging and EDS element mapping indicated a homogeneous distribution of Eu, Ca, and Ti throughout the polycrystalline sample, and the actual Eu:Ca ratio agreed well with the nominal stoichiometry. Measurements of magnetic susceptibility vs. temperature indicated antiferromagnetic ordering in samples with $x \leq 0.60$, with T_N decreasing from 5.4 K in $EuTiO_3$ to 2.6 K in $Eu_{0.40}Ca_{0.60}TiO_3$. No antiferromagnetic ordering above 1.8 K was detected in samples with $x > 0.60$.

1. Introduction

Europium titanate, $EuTiO_3$, crystallizes in the cubic perovskite structure [1] and is classified as a paraelectric/antiferromagnetic (PE/AFM) material. The localized $4f$ electrons on the Eu atoms order antiferromagnetically below $T_N=5.5$ K, adopting a G-type arrangement with each nearest neighbor Eu spin aligned antiparallel [2]. Recently, it was observed that the magnetic and dielectric properties of $EuTiO_3$ are coupled. Studies have shown that the localized spins are strongly coupled to an IR-active phonon mode [3], and theoretical predictions [4] suggest that a modest biaxial compressive strain of 1.2% could force a transition from a PE/AFM state to a ferroelectric/ferromagnetic (FE/FM) state. This suggests that epitaxial strain can be used to induce multiferroic behavior in $EuTiO_3$. Subsequent studies of $EuTiO_3$ deposited on lattice-matched $SrTiO_3$ have yielded interesting results [5–7], including a report of ferromagnetism with a Curie temperature (T_c) of 5 K in oxygen-deficient thin films [6] and the persistence of antiferromagnetism in unstrained stoichiometric thin films [7].

An alternative strategy for mimicking the effects of compressive strain in bulk powders of $EuTiO_3$ is through chemical substitution. For example, Ca^{2+} is smaller than Eu^{2+}, so substituting Ca^{2+} for Eu^{2+} in $Eu_{1-x}Ca_xTiO_3$ should result in a decrease of unit cell length and a net contraction of the structure. A previous report describing substitution of the larger Ba^{2+} cation for Eu^{2+} in $Eu_{1-x}Ba_xTiO_3$ ($0 \leq x \leq 0.2$) showed that the unit cell length expanded as expected, but resulted in a decrease in coupling between the magnetism and the dielectric constant due to dilution effects and increased disorder [8]. However, the effects of substitution with the smaller Ca^{2+} cation have not been studied. In this paper, we describe a solution precursor route that facilitates the synthesis of several members of the $Eu_{1-x}Ca_xTiO_3$ solid solution across the entire composition range from $EuTiO_3$ ($x=0$) to $CaTiO_3$ ($x=1$). Specifically, a modified sol–gel process was used to form $Ca^{2+}–Eu^{3+}–Ti^{4+}–O^{2-}$ precursors with homogeneous mixing of the elements, followed by reductive annealing to generate $Eu_{1-x}Ca_xTiO_3$ with $0 \leq x \leq 1$. Increasing substitution of Ca^{2+} for Eu^{2+} results in a smooth decrease in lattice constant and a suppression of antiferromagnetic ordering, which is correlated to the structure and composition.

2. Experimental section

2.1. Materials

The following chemicals were used: Eu_2O_3 (99.9%, Alfa Aesar), $CaCO_3$ (99.95%, Alfa Aesar), titanium isopropoxide

* Corresponding author at: Department of Chemistry, The Pennsylvania State University, University Park, PA 16802, USA.
E-mail address: schaak@chem.psu.edu (R.E. Schaak).

Table 1
Synthesis details for $Eu_{1-x}Ca_xTiO_3$.

Nominal x in $Eu_{1-x}Ca_xTiO_3$	Mass of Eu_2O_3 (g)	Mass of $CaCO_3$ (g)	Volume of $Ti(iOPr)_4$ (mL)
0.00	0.4959	0.0000	1.215
0.05	0.4710	0.0200	1.230
0.10	0.4462	0.0402	1.215
0.15	0.4209	0.0602	1.215
0.25	0.3717	0.1001	1.215
0.35	0.3219	0.1400	1.215
0.50	0.2480	0.2001	1.215
0.55	0.2232	0.2200	1.215
0.60	0.1984	0.2398	1.215
0.65	0.1737	0.2601	1.215
0.80	0.0993	0.3203	1.215
1.00	0.0000	0.2000	0.605

$(Ti(OCH(CH_3)_2)_4$ or $Ti(iOPr)_4$, 97%, Alfa Aesar), and HNO_3 (70%, 16 M). All chemicals were used as purchased without further modification except Eu_2O_3, which was fired at 1000 °C for 3 h prior to use in order to remove carbonate impurities for accurate weighing.

2.2. Synthesis

Samples were synthesized using a modified sol–gel approach [9] followed by annealing under reducing conditions. For the synthesis of phase pure $EuTiO_3$, a 35 mmol Eu^{3+} solution was prepared by adding Eu_2O_3 to a 10:1 mixture of ethanol and HNO_3 and stirring until the solution became clear. A stoichiometric amount of $Ti(iOPr)_4$ was added dropwise to the reaction, resulting in a clear orange solution. The solution was allowed to stir for at least 3 h or overnight, and the solvent was removed by heating to ~80 °C, yielding a pale orange powder. The resulting powder was annealed under flowing H_2/Ar (5%/95%) at 1000 °C for 12 h in order to reduce Eu^{3+} to Eu^{2+}, yielding a black powder ($EuTiO_3$). ($EuTiO_3$ begins to form at temperatures as low as 700 °C, but complete reduction of Eu^{3+} to Eu^{2+} and the concomitant formation of phase-pure $EuTiO_3$ requires heating to 1000 °C.) For the synthesis of Ca-substituted $EuTiO_3$, stoichiometric amounts of $CaCO_3$ were added to the initial Eu^{3+} solution and allowed to dissolve completely before addition of the $Ti(iOPr)_4$. The resulting powders were processed under identical conditions as described for $EuTiO_3$. Table 1 lists the exact amounts of Eu_2O_3, $CaCO_3$, and $Ti(iOPr)_4$ that were used to synthesize each sample. Typical sample sizes were 0.5–1.0 g of product.

2.3. Characterization

Powder XRD data were collected using a Bruker D8 Advance Diffractometer with a LynxEye 1D detector (Cu$K\alpha$ radiation). XRD patterns were obtained from powdered samples at room temperature and lattice parameters were refined using Chekcell. Scanning electron microscopy (SEM), energy dispersive X-ray spectroscopy (EDS), and EDS element mapping were performed using a JEOL JSM 5400 SEM operating at 20 kV. EDS data for all samples were collected for at least 5–10 min, and collection of multiple data points from the same samples confirmed standard deviations within 3–5%. Magnetic characterization was performed using a Quantum Design SQUID magnetometer. The reported Curie–Weiss temperatures (θ_W) were obtained directly from the slopes of the Curie–Weiss plots ($1/\chi$ vs. T) in the temperature range of $10 K < T < 25 K$, which were linear for all samples (see Electronic Supplementary Information). These values quanti-

tatively match those derived from higher temperature data ($25 K < T < 100 K$).

3. Results and discussion

Bulk powders of mixed-metal oxides are typically synthesized using standard high-temperature ceramic methods. For the case of perovskite-type $EuTiO_3$ with Eu^{2+} and Ti^{4+} [10], bulk powders have previously been synthesized by the reaction of Eu_2O_3 and TiO_2 [11] as well as through the reductive annealing of
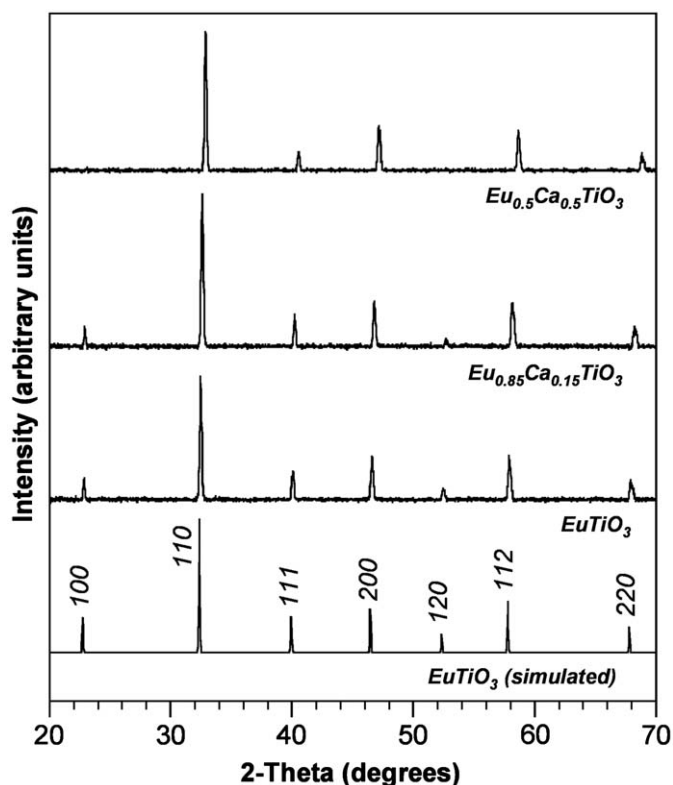

Fig. 1. Powder XRD patterns for $EuTiO_3$, $Eu_{0.85}Ca_{0.15}TiO_3$, and $Eu_{0.5}Ca_{0.5}TiO_3$. The simulated powder XRD pattern for $EuTiO_3$ is shown for comparison.
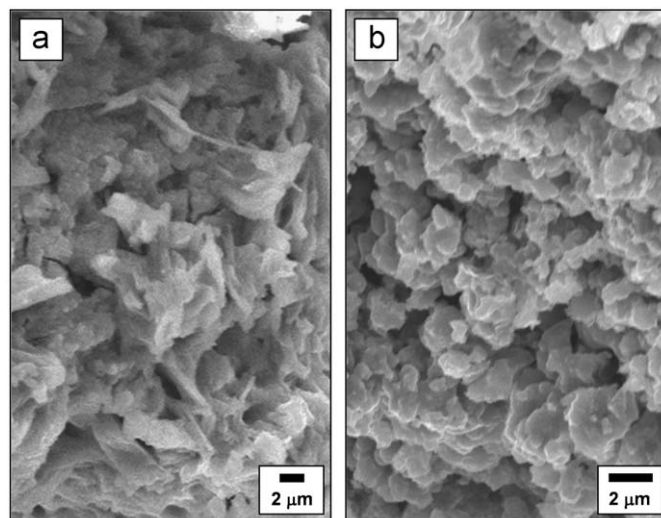

Fig. 2. SEM images of (a) the sol–gel precursor and (b) the final crystalline product for $EuTiO_3$.

mechanochemically activated Eu_2O_3 and TiO_2 [12]. Solution precursor methods provide an alternative strategy for ensuring homogeneous mixing of multiple elements, particularly for chemically substituted phases where stoichiometry control at low concentrations is important. Accordingly, we applied a modified sol–gel approach to the synthesis of $EuTiO_3$ and a wide range of chemically substituted members of the $Eu_{1-x}Ca_xTiO_3$ solid solution. This process has been used previously to synthesize similar perovskite phases such as Eu^{3+}-doped zirconates [13] and Pr^{3+}-doped $CaTiO_3$ [14], but to the best of our knowledge has not been applied to divalent lanthanide oxides such as $EuTiO_3$.

Powder XRD data for a typical sample of $EuTiO_3$ are shown in Fig. 1, along with simulated XRD data for comparison. The solution precursor route yields perovskite-type $EuTiO_3$ with no

Table 2
Eu:Ca stoichiometries and refined lattice constants for $Eu_{1-x}Ca_xTiO_3$.

Nominal x in $Eu_{1-x}Ca_xTiO_3$	Actual x in $Eu_{1-x}Ca_xTiO_3$ (EDS)	Lattice constant (a, Å)
0.00	0.00	3.902(3)
0.05	0.05	3.895(2)
0.10	0.09	3.891(2)
0.15	0.14	3.885(2)
0.25	0.22	3.878(1)
0.35	0.33	3.871(1)
0.50	0.48	3.857(3)
0.55	0.51	3.848(2)
0.60	0.56	3.845(2)
0.65	0.61	3.843(2)
0.80	0.79	3.829(1)[a]
1.00	1.00	3.807(7)[a]

[a] Although $CaTiO_3$ has an orthorhombic supercell at room temperature, the subunits are related to the simple perovskite unit cell and can be analyzed accordingly for purposes of comparison. Thus, the pseudocubic lattice parameters for $CaTiO_3$ and the $Eu_{1-x}Ca_xTiO_3$ samples with high Ca contents were calculated based on the simple cubic structure of $EuTiO_3$.
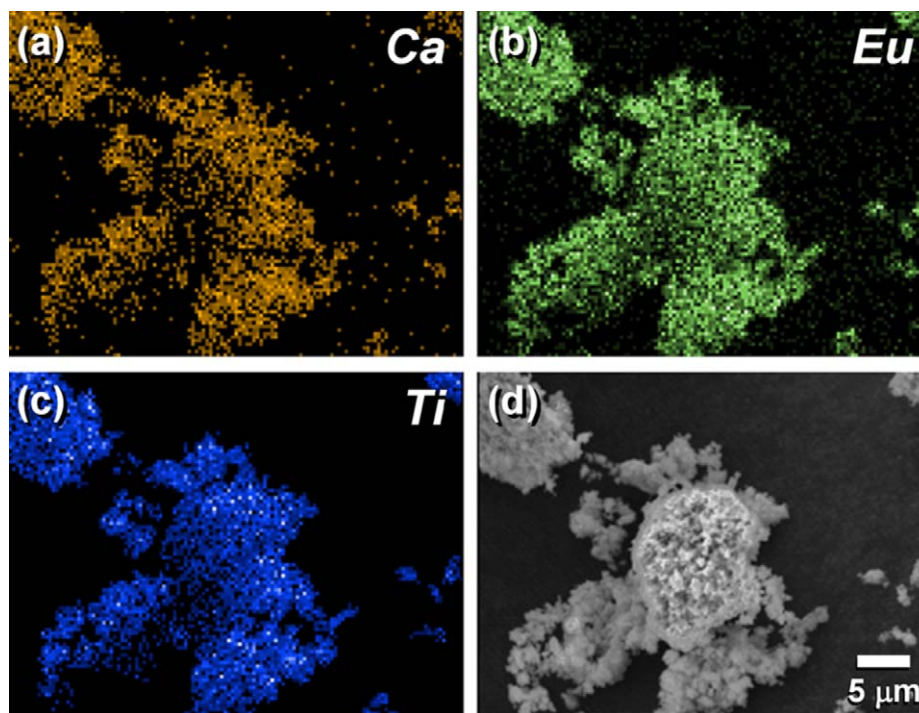
evidence of crystalline impurities. An observed weight gain upon thermal gravimetric analysis in oxygen indicates that a small amount of Eu^{3+} is present, most likely as an amorphous $EuTiO_x$ phase as observed previously [15]. EDS data show a 47:52 ratio of Eu:Ti, which is consistent (within experimental error) with the nominal stoichiometry. An SEM image of the $EuTiO_3$ powder (Fig. 2) shows that the particles are micron-sized and not densely compacted. The morphology of the $EuTiO_3$ product is related to that of the sol–gel precursor, also shown in Fig. 2. Fig. 1 also shows XRD data for two representative members of the $Eu_{1-x}Ca_xTiO_3$ solid solution: $Eu_{0.85}Ca_{0.15}TiO_3$ and $Eu_{0.50}Ca_{0.50}TiO_3$. EDS data (Table 2) confirm the expected Ca:Eu stoichiometry in both samples. The SEM image and corresponding EDS element mapping data for another representative sample, $Eu_{0.75}Ca_{0.25}TiO_3$ (Fig. 3), confirms the homogeneous distribution of Ca, Eu, and Ti throughout the sample.

Fig. 4 shows powder XRD data for all synthesized members of the $Eu_{1-x}Ca_xTiO_3$ solid solution: $x=0.00$, 0.05, 0.10, 0.15, 0.25, 0.35, 0.50, 0.55, 0.60, 0.65, 0.80, and 1.00. All appear by laboratory XRD to have only one crystalline phase present, except for the samples with $x=0.65$, 0.80, and 1.00, which have small amounts of rutile TiO_2 impurities. Comparison with the peak positions for pure $EuTiO_3$ shows a smooth progression of lattice contraction upon substitution of Ca^{2+} for Eu^{2+}, indicating that this is indeed an effective strategy for composition tuning through the $Eu_{1-x}Ca_xTiO_3$ solid solution. Relevant data for the $Eu_{1-x}Ca_xTiO_3$ samples are collected in Table 2, including the refined lattice constants and the approximate value of x in $Eu_{1-x}Ca_xTiO_3$ (as determined by EDS). The lattice constants and unit cell volumes contract as the amount of Ca^{2+} increases, as expected.

Fig. 5 presents a plot of lattice constant vs. composition, which shows good agreement with Vegard's law and further confirms the facile formation of a complete $Eu_{1-x}Ca_xTiO_3$ solid solution. At room temperature, $CaTiO_3$ is orthorhombic with a $\sqrt{2} \times \sqrt{2} \times 2$ supercell that results from cooperative distortions of the TiO_6 octahedra. For the $Eu_{1-x}Ca_xTiO_3$ samples with $x > 0.65$, the onset

Fig. 3. EDS element mapping data for $Eu_{0.75}Ca_{0.25}TiO_3$ highlighting the homogeneous distribution of (a) Ca, (b) Eu, and (c) Ti throughout the sample. The corresponding SEM image is shown in (d).
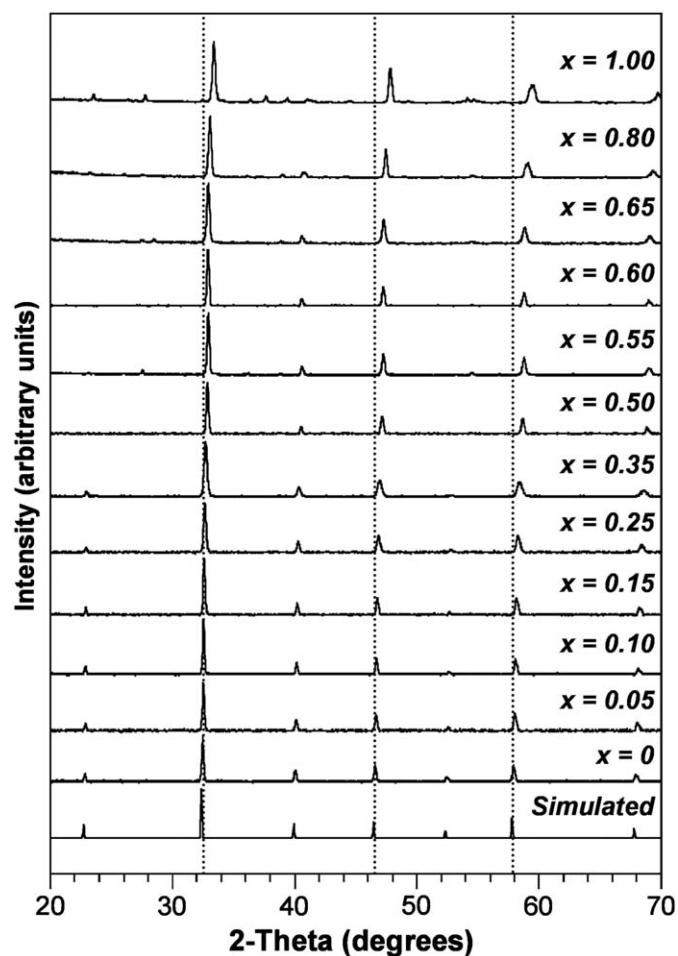
Fig. 4. Powder XRD data for all synthesized members of the $Eu_{1-x}Ca_xTiO_3$ solid solution, including the end members $EuTiO_3$ and $CaTiO_3$. The simulated XRD pattern for $EuTiO_3$ is shown for comparison. The dotted vertical lines highlight the shift in peak positions to higher angles upon substitution of Ca^{2+} for Eu^{2+}. Small TiO_2 impurity peaks occur in some of the samples at 27.7, 36.6, 57.3, and 64.8° 2θ.
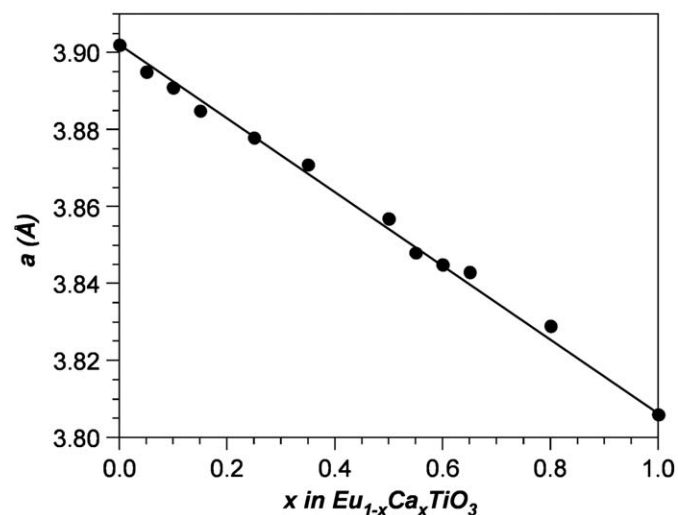

Fig. 5. Plot of lattice constant vs. composition for all synthesized members of the $Eu_{1-x}Ca_xTiO_3$ solid solution, which shows good agreement with Vegard's law (solid line).

cubic-to-orthorhombic transition has not been probed in detail, however, so we cannot rule out the possibility that a tetragonal phase appears near the changeover [16]. For purposes of comparison, particularly for comparing unit cell contraction upon substituting Ca^{2+} for Eu^{2+}, all of the $Eu_{1-x}Ca_xTiO_3$ samples were treated as cubic or pseudocubic (ignoring the supercell of $CaTiO_3$) and analyzed accordingly based on the simple perovskite subcell. This approach has been shown to be an effective way of comparing compounds in related systems, such as cubic $EuTiO_3$ vs. other $RETiO_3$ (RE=rare earth) phases with orthorhombic supercells [11]. Similar results were obtained by fitting the orthorhombic patterns with an orthorhombic cell to determine the unit cell volume, then relating the volume back to the cubic lattice constant (e.g. 3.807 Å vs. 3.804 Å for $CaTiO_3$,
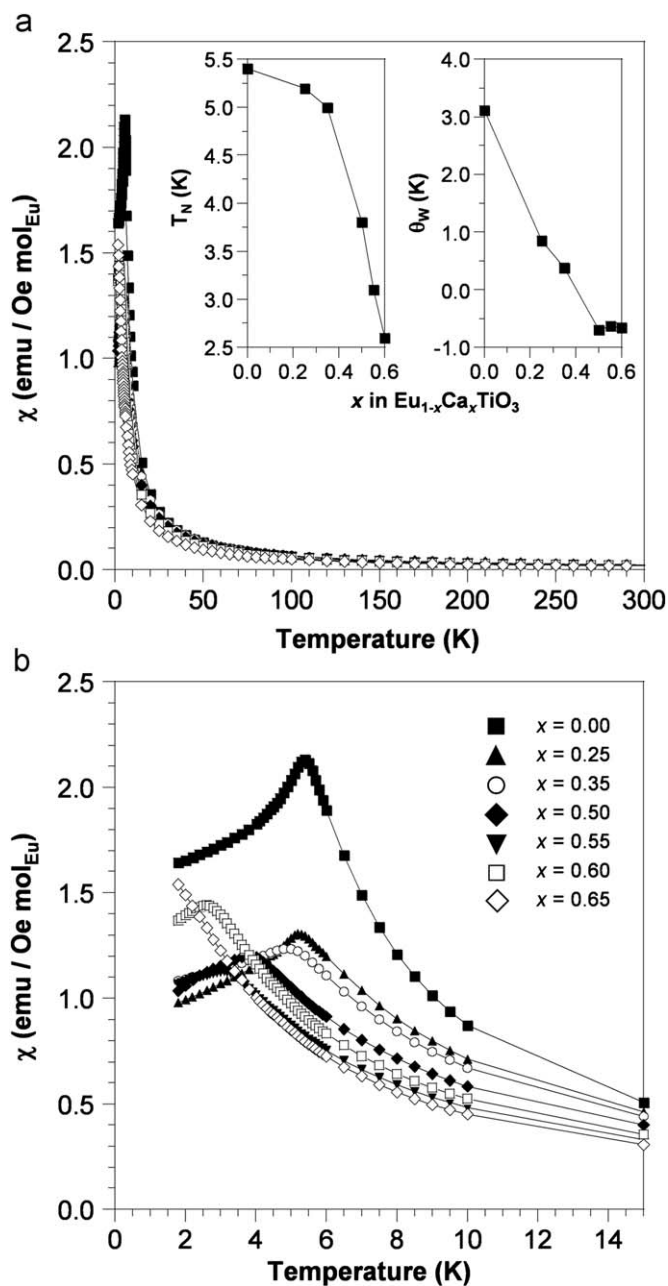

Fig. 6. Plots of magnetic susceptibility (χ) vs. temperature at 100 Oe for representative $Eu_{1-x}Ca_xTiO_3$ samples. Panel (a) shows χ vs. T from 300 to 1.8 K, along with plots of T_N vs. composition and θ_W vs. composition (x in $Eu_{1-x}Ca_xTiO_3$) for the samples that order antiferromagnetically above 1.8 K. Panel (b) shows an expanded view of χ vs. T from 15 to 1.8 K. The legend for both panels is included in (b).

of slight broadening and asymmetry in the high angle diffraction peaks are consistent with the orthorhombic structure of $CaTiO_3$, while samples with $x \leq 0.65$ match the cubic cell of $EuTiO_3$. This

which are equivalent within the standard deviation presented in Table 2).

Fig. 6 shows plots of magnetic susceptibility vs. temperature for a representative group of $Eu_{1-x}Ca_xTiO_3$ samples: x=0.00, 0.25, 0.35, 0.50, 0.55, 0.60, and 0.65. $EuTiO_3$, as expected, is antiferromagnetic with T_N=5.4 K. As the Eu^{2+} is progressively substituted with non-magnetic Ca^{2+}, T_N decreases. For $Eu_{0.75}Ca_{0.25}TiO_3$ and $Eu_{0.65}Ca_{0.35}TiO_3$, T_N=5.2 and 5.0 K, respectively. T_N decreases more abruptly to 3.8, 3.1, and 2.6 K for $Eu_{0.50}Ca_{0.50}TiO_3$, $Eu_{0.45}Ca_{0.55}TiO_3$, and $Eu_{0.40}Ca_{0.60}TiO_3$, respectively. For samples with $x \geq 0.65$, antiferromagnetic ordering was not observed above 1.8 K. Fig. 6 also shows a plot of the Curie–Weiss temperature (θ_W, derived from the Curie–Weiss fit from approx. 10–25 K) as a function of x in $Eu_{1-x}Ca_xTiO_3$. Interestingly, the Curie–Weiss temperature decreases dramatically at small values of x, indicating a significant decrease in magnetic exchange interaction with dilution, despite the fact that T_N decreases only slightly as discussed above. The Curie–Weiss temperature drops to small negative values when x is large, consistent with the large suppression of T_N, and the qualitative difference between the two quantities may be understood as the result of competing contributions to the Curie–Weiss fit. Taken together, the data indicate that the substitution of Ca^{2+} for Eu^{2+} at a level needed to induce significant lattice compression suppresses antiferromagnetism in $EuTiO_3$, presumably the result of significant magnetic dilution that decreases the spin–spin interactions. Thus, the magnetic phase transition predicted in $EuTiO_3$ thin films due to epitaxial strain [4] is not seen in these magnetically diluted bulk materials.

4. Conclusions

In this paper, we have synthesized and characterized 12 members of the $Eu_{1-x}Ca_xTiO_3$ solid solution, including the end members $EuTiO_3$ and $CaTiO_3$. A modified sol–gel precursor route facilitates homogeneous mixing of Eu^{3+} and Ca^{2+}, and reductive annealing generates Eu^{2+} and forms the $Eu_{1-x}Ca_xTiO_3$ products. Substitution of Ca^{2+} for Eu^{2+} progressively decreases T_N from 5.4 K in $EuTiO_3$ to 2.6 K in $Eu_{0.40}Ca_{0.60}TiO_3$, ultimately suppressing long-range antiferromagnetic ordering above 1.8 K for $Eu_{1-x}Ca_xTiO_3$ samples with $x \geq 0.65$. While the large amount of Ca^{2+} necessary to induce significant lattice compression compromises the long-range coupling between the magnetic Eu^{2+} ions due to magnetic dilution effects, this continuous solid solution could serve as an interesting model system for more detailed studies of magnetic dilution effects and magnetic clusters within non-magnetic solids [17].

Appendix A. Supplementary material

Supplementary data associated with this article can be found in the online version at doi:10.1016/j.jssc.2009.12.025.

References

[1] J. Brous, I. Fankuchen, E. Banks, Acta Crystallogr. 6 (1953) 67–70.
[2] [a] T.R. McGuire, M.W. Shafer, R.J. Joenk, H.A. Alperin, S.J. Pickart, J. Appl. Phys. 37 (1966) 981–982;
[b] R. Ranjan, H.S. Nabi, R.J. Pentcheva, J. Phys. Condens. Matter 19 (2007) 406172.
[3] [a] T. Katsufuji, H. Takagi, Phys. Rev. B 64 (2001) 054415;
[b] Q. Jiang, H. Wu, J. Appl. Phys. 93 (2003) 2121–2125.
[4] C.J. Fennie, K.M. Rabe, Phys. Rev. Lett. 97 (2006) 267602.
[5] K. Fujita, N. Wakasugi, S. Murai, Y. Zong, K. Tanaka, Appl. Phys. Lett. 94 (2009) 062512.
[6] K. Kugimiya, K. Fujita, K. Tanaka, K. Hirao, J. Magn. Magn. Mater. 310 (2007) 2268–2270.
[7] J.H. Lee, X. Ke, N.J. Podraza, L. Fitting Kourkoutis, T. Heeg, M. Roeckerath, J.W. Freeland, C.J. Fennie, J. Schubert, D.A. Muller, P. Schiffer, D.G. Schlom, Appl. Phys. Lett. 94 (2009) 212509.
[8] H. Wu, Q. Jiang, W.Z. Shen, Phys. Rev. B 69 (2004) 014104.
[9] M.P. Pechini, US Patent 3, 330, 697, July 11, 1967.
[10] A.H. Morrish, J. Appl. Phys. 36 (1965) 1145–1152.
[11] G.J. McCarthy, W.B. White, R. Roy, Mater. Res. Bull. 4 (1969) 251–256.
[12] S. Kamba, D. Nuzhnyy, P. Vanek, M. Savinov, K. Knizek, Z. Shen, E. Santava, K. Maca, M. Sadowski, J. Petzelt, Europhys. Lett. 80 (2007) 27002.
[13] H. Zhang, X. Fu, S. Niu, Q. Xin, J. Alloys Compd. 459 (2008) 103–106.
[14] X. Zhang, J. Zhang, X. Zhang, M. Wang, H. Zhao, S. Lu, X.-J. Wang, J. Phys. Chem. C 111 (2007) 18044–18048.
[15] N.L. Henderson, J. Baek, P.S. Halasyamani, R.E. Schaak, Chem. Mater. 19 (2007) 1883–1885.
[16] Q. Zhou, B.J. Kennedy, J. Solid State Chem. 179 (2006) 3568–3574.
[17] [a] H. Maletta, G. Crecelius, J. Magn. Magn. Mater. 6 (1977) 107–110;
[b] S.M. Yunus, F.U. Ahmed, M.A. Asgar, J. Alloys Compds. 315 (2001) 90–94.